Causal Relationships Underlying Episodic Memory Network Dynamics in Older Adults

Abbreviated title: Causal Network Dynamics in Aging

Simon W. Davis[1, 2, 3], Bruce Luber[2], David L.K. Murphy[2], Sarah H. Lisanby[2], Roberto Cabeza[1]

[1]Center for Cognitive Neuroscience, Duke University, 27708; [2]Division of Brain Stimulation, Department of Psychiatry and Behavioral Sciences, Duke University School of Medicine, 27708; [3]Department of Neurology, Duke University School of Medicine, 27708.

Corresponding author:
Simon W Davis
Department of Neurology
Box 2900, DUMC
Duke University
Durham, NC 27708
simon.davis@duke.edu

Pages: 34
Tables: 1
Figures: 7

Words: Abstract: 244; Introduction: 647; Discussion: 1455.

COI: No COI.
Acknowledgements: This work was supported by National Institutes of Health Grant R01 AG19731.

Abstract

The most reliable finding in functional neuroimaging studies of cognitive aging is a more widespread brain activity pattern in older than younger adults. The additional regions recruited by older adults are functionally connected to core task-network regions, and frequently contribute to task performance in this group, suggesting that older adults may compensate for core task-network deficits by expanding the task-related network. This hypothesis is difficult to resolve with functional neuroimaging alone, because it is unclear both how to define reliable causal trends in which connections are important (e.g., local versus indirect connections). To address this problem we examined functional connectivity measures as quantified by a region's local *within-module degree* (WMD), or their *between-module degree* (BMD) between distant cortical communities. We combined these graph theoretical measures with diffusion tensor imaging (DTI) and repetitive transcranial magnetic stimulation (rTMS) in order to resolve the central hypothesis. We applied enhancing (5Hz) or impairing (1Hz) rTMS to a core episodic encoding region, the left prefrontal cortex (PFC) and predicted that (1) if older adults compensate for local deficits by boosting BMD, then enhancing left PFC function should reduce BMD, whereas impairing it, should increase BMD and (2) that this effect should be correlated with DTI measures of white-matter integrity. Both predictions were confirmed, supporting for the compensatory interpretation of an expanded task network in older adults. More generally, the results illustrate the power of combining rTMS with functional and structural connectivity measures to investigate age-related changes in network architecture.

Significance Statement

An integrated account of the functional dynamics of cortical connectivity in aging is incomplete. Our approach is to unite network theory, brain stimulation, and diffusion tractography in order determine how the aging brain adapts to local changes in cortical reactivity during episodic encoding. We found that aging brains adapt their local and distal connectivity patterns in a frequency-selective manner, and that these changes are constrained by white matter connectivity. These results help to advance a mechanistic understanding of the network dynamics associated with episodic memory performance, and suggest novel interventions to improve memory functioning in later adulthood.

Introduction

In functional neuroimaging studies of cognitive aging, older adults (OAs) frequently show display a more widespread pattern of brain activity than young adults (YAs). This effect is often takes the form of an age-related reduction in core task-network regions coupled with an increase in secondary task-network areas (Nyberg et al., 2010; Davis et al., 2014). During verbal episodic memory encoding tasks, for example, OAs frequently show weaker activity in the left PFC, a key verbal encoding region, but stronger activity in right PFC (Persson et al., 2006; Cox et al., 2015; Proskovec et al., 2016), a region rarely recruited during verbal encoding by YAs (Spaniol et al., 2009). PFC regions over-recruited by OAs often show stronger long-range functionally connectivity outside of local cortical communities (Geerligs et al., 2015) and an association with successful cognitive performance in this group (Dennis et al., 2008; Spaniol and Grady, 2012). We and others have suggested that OAs compensate for regional deficits by expanding the task-related network via long-range connectivity (Antonenko et al., 2012; Davis et al., 2012). Our approach to these questions is therefore to unite network theory, brain stimulation, and diffusion tractography, in order determine how the aging brain adapts to local inhibition of cortical reactivity.

We propose and test a new hypothesis based on the graph-based concept of modularity (Chang et al., 2012). Modularity refers a network architecture where groups of nodes communicate more intimately with each other than with other nodes in the network. A modular network requires both *within-module degree* (WMD) and *between-module degree* (BMD). WMD represents the sum of local connectivity within a cortical community, whereas BMD describes the sum of connectivity based on inputs from other modules). Using these ideas, we proposed a hypothesis of widespread activation pattern and increase in long-range functional connectivity displayed by OAs. We hypothesize that *OAs compensate for a deficit in core network regions by relying on between module*

connections (BMD) when local resources are depleted through a causal brain stimulation manipulation.

Noninvasive brain stimulation technologies offer a unique opportunity to probe this functional and structural reorganization to resolve the functional relevance of network structure in aging. Transcranial magnetic stimulation (TMS) at low frequencies (e.g., 1Hz) has been shown to reliably depress local hemodynamic activity (de Vries et al., 2012) and impairs cognitive performance associated with the local region. If the age-related increase in distal connectivity patterns reflects a compensatory phenomenon, we would expect this 1Hz TMS to induce an increase in distal connectivity associated with successful memory. Conversely, 5Hz TMS has been found in induce local *increases* in BOLD reactivity (Schneider et al., 2010) and should promote greater local connectivity associated with successful task performance.

In the current study, we use rTMS to test two predictions. First, we directly manipulate the hypothetical cause of the compensatory change, i.e., the operation of a task-related brain region. Using rTMS we either impair (1Hz) or enhance (5Hz) the function of core region for verbal episodic memory encoding: left PFC. We predict that *impairing left PFC function will increase BMD between distant PFC regions, whereas enhancing its function will increase WMD with the stimulation site* (Prediction 1). Second, given that functional connectivity depends on structural connectivity (Gong et al., 2009), it follows that TMS-related changes in WMD or BMD are constrained by the quality of white-matter tractography between nodes in a network. Therefore, *we predict that while WMD will be correlated with direct structural connections with the stimulation site, BMD will be related to indirect structural connectivity* (*Prediction 2*). We delivered 1Hz and 5Hz rTMS immediately before scanning while encoding sentences, in order to promote distal and local functional connectivity increases, respectively. The first prediction was tested by comparing the two rTMS conditions on WMD and BMD and the second, by

correlating BMD with structural distance measures. The confirmation of the two predictions would directly support our account of widespread activity in OAs.

Materials & Methods

Participants

Fourteen healthy older adults were recruited for this study (all native English speakers; 7 females; age mean +/- SD, 66.7 +/- 3.9 years; range 61-74 years); one subject was subsequently removed from the analysis due to tolerability during rTMS. Each older adult was screened for exclusion criteria for TMS (history of seizure, brain/head injuries) as well as psychiatric condition (MINI International Neuropsychiatric Interview, English Version 5.0.0 DSM-IV, Sheehan et al., 2006). None of the older participants reported subjective memory complaints in everyday life or had MMSE score below 27 (mean +/- SD = 29.1 +/- 0.8).

Stimuli

The source memory task was comprised of a set of sentences which included a concrete subject and direct object. In each sentence, both subject and direct object were capitalized to indicate to the subject which specific nouns were to be remembered (*"A SURFBOARD was on top of the TRUCK."*). Associative strength between nouns in a sentence (as determined by the USF word association norms (Nelson et al., 2004)), were normally distributed, and both the imageability, frequency, and total length of each set of sentences was counterbalanced across all sentences used therein.

Image Acquisition

An outline of all data acquisition events is depicted in **Figure 1**. Scanning was divided between two days, 1-4 days apart, with the first day comprised of a functional memory-success localizer for scanning and stimulation on Day 2. All procedures were completed

on a GE MR 750 3-Tesla scanner, with a single channel (to allow space to insert the TMS coil).

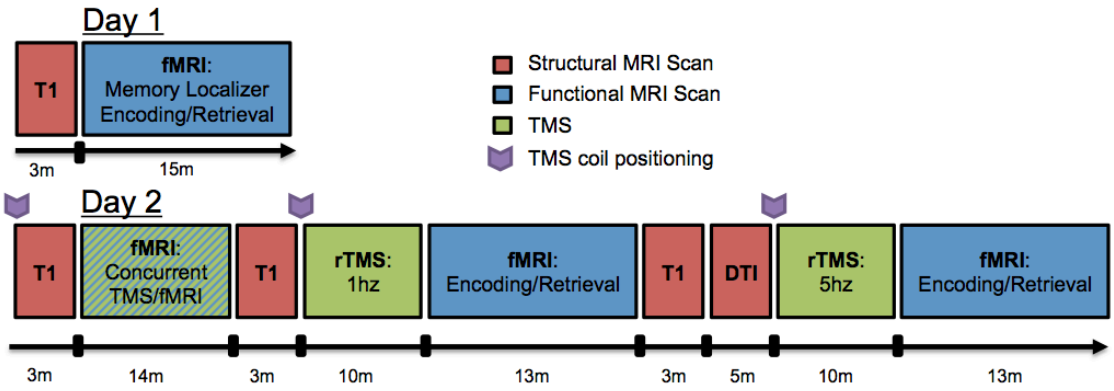

Figure 1. Data acquisition schedule.

TMS Procedure

Prior to the TMS-fMRI session, the scalp location for TMS coil position over the left middle frontal gyrus (MFG) location had been found by using an infrared neuronavigation system (Brainsight: Rogue Research, Montreal, Canada). Specifically, the point of greatest activation in the left MFG in the fMRI memory contrast (i.e., encoding trials which were subsequently remembered versus forgotten) from the first day of scanning was chosen from the fMRI overlay on the subject's structural MRI, both of which had been uploaded into BrainSight. After co-registration of the subject's head with his MRI, the MFG location was marked on a tight fitting acrylic swim cap that stayed on the subject's head until TMS-fMRI interleaving was completed on the same day. At that time, subjects were acclimated to the sort of TMS pulses to be delivered later in the scanner with a series of single pulses at the target site, as well as a short burst of 5Hz stimulation. The motor threshold (MT) for each subject was determined using a MagVenture R30M device located outside the scanner room, part of an MRI compatible

TMS system which included a non-ferrous figure-8 coil with 12m long cable and artifact reducing counter-current charging system (MagVenture, Farum, Denmark). MTs were determined using electromyography of the right first dorsal interosseous (FDI) muscle and defined as the lowest setting of TMS device intensity at which ≥ 5 out of 10 motor evoked potentials of at least 50μV peak to peak amplitude could be elicited. The TMS coil was then positioned over the individual's marked left MFG target site and locked into place using a coil holder provided as part of the MagVenture system, and subjects were then positioned in the bore of the MR scanner.

For rTMS, two 10-minute trains of either 1Hz or 5Hz stimulation were delivered at 120% MT immediately prior to a fMRI acquisition. The position of the TMS coil was reset to the same target site before the beginning of each rTMS session, and monitored continuously while the subject lay supine in the bed of the MR scanner. 1Hz rTMS was delivered in a continuous train of 10 minutes, while 5Hz rTMS was delivered in intermittent 6 sec trains with a 24 sec inter-train interval, also for 10 minutes. Thus, dosage was equivalent between 1Hz and 5Hz rTMS conditions (600 total pulses), and the order of stimulation type was counterbalanced across subjects. Immediately after the 10 minutes of TMS, subjects were positioned in the scanner, and performed the encoding portion of the sentence task while fMRI was acquired.

Data Analyses

The general analytical pipeline is depicted in **Figure 2**. Briefly, both functional and structural imaging data were processed according to standard preprocessing heuristics (see below), and adjacency matrices comprising psychophysiological interaction (PPI)-based functional correlations associated with the task (fMRI data) or structural connections based on tractography streamline counts (DWI data) were evaluated. Modularity was based solely on structural connectivity, and regions within a high-

dimensional atlas (n = 471 regions) were partitioned using conditional expected models (Chang et al., 2012). In order to compare functional and structural networks we use graph-theoretical methods to find the distance traversed by the lowest weighted path in a structural network, which is constructed by connecting each cortical region with a weighted edge. We proceed stepwise, by relating our functional network $\boldsymbol{A_{fMRI}}$ to our structural network $\boldsymbol{A_{DTI}}$, at structural paths of length $\boldsymbol{l}$, by which we are able to demonstrate the value of both local (direct) and long-distance (indirect) paths in promoting success-related connectivity.

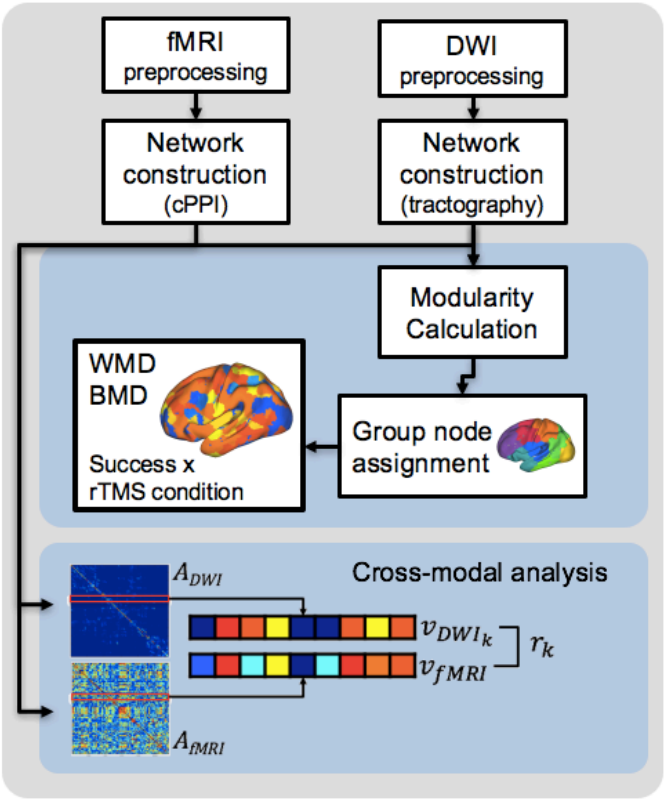

Figure 2. Analytical pipeline. Schematic depicts the general analytic pipeline used in the current study, both functional and structural imaging data were processed according to standard preprocessing heuristics (see Material & Methods), and adjacency matrices comprising functional correlation associated with the task (fMRI data) or structural connections based on streamline counts (DWI data) were evaluated. Then, both structural and functional matrices are submitted to a modular decomposition. Next, the modal decomposition across all subjects is used to describe the most common modular breakdown (in the baseline Encoding Success (DM) condition). Within-module degree (WMD) and between-module degree (BMD) are then computed for each subject using these modular assignments. Lastly, cross-modal analyses are completed

by calculating the Pearson's product moment correlation r_k, based on two vectors representing diffusion tractography at each step size k (v_{DWI_k}) and functional connectivity (v_{fMRI}) information drawn from structural or functional networks A_{DWI_k} or A_{fMRI}, respectively.

Structural and functional preprocessing

Diffusion-weighted images were preprocessed using typical methods, including brain extraction, correction for eddy-current distortion and simple head motion, and correction of the b-matrix for any rigid-body coregistration completed in this step (Smith et al., 2006). Fractional anisotropy (FA) images were generated using the tensor model from *dtifit* (FSL, www.fmrib.ox.ac.uk/fsl/). The preprocessing of functional data for both the baseline, and post-rTMS conditions was carried out using image processing tools from FSL 5.01 (FMRIB, Oxford, UK). Images were corrected for slice acquisition timing, motion, and linear trend; temporally smoothed with a high-pass filter using a 190s cutoff; and normalized to the Montreal Neurological Institute (MNI) stereotaxic space. Spatial filtering with a Gaussian kernel of full-width half-maximum (FWHM) of 6mm was applied. Voxel time-series analysis was carried out using general linear modeling (GLM); fixed effects models were carried out to examine the effects of 1) both memory success and stimulation frequency in the baseline and post-rTMS data. We modeled encoding trials that were either subsequently remembered or subsequently forgotten, in order to examine standard subsequent memory effects (SMEs) in the baseline, post-1Hz rTMS, and post-5Hz rTMS runs.

Construction of connectivity matrices

Before either structural or functional matrices were constructed, we first sought to establish a consistent parcellation scheme across all image types that reflects an accurate summary of full connectome effects (Bellec et al., 2015). Subjects' T1-weighted images were segmented using the SPM12 (www.fil.ion.ucl.ac.uk/spm/software/spm12/),

yielding a grey matter (GM) and white matter (WM) mask in the T1 native space for each subject. The entire GM was then parcellated into 471 regions of interest (ROIs), each representing a network node by using a subparcellated version of the Harvard-Oxford Atlas, (Tzourio-Mazoyer et al., 2002), defined originally in MNI space. The T1-weighted image was then nonlinearly normalized to the ICBM152 template in MNI space using fMRIB's Non-linear Image Registration Tool (FNIRT, FSL, www.fmrib.ox.ac.uk/fsl/). The inverse transformations were applied to the HOA atlas in the MNI space, resulting in native-T1-space GM parcellations for each subject. Then, T1-weigted images were coregistered to native diffusion space using the subjects' unweighted diffusion image as a target; this transformation matrix was then applied to the GM parcellations above, resulting in a native-diffusion-space parcellation for each subject.

For structural connection matrices, network edges were defined by the number of tractography streamlines between any two ROIs. We used Dipy (Garyfallidis et al., 2014) to fit the data with the constant solid angle (CSA) model with fourth-order spherical harmonics, and generating generalized FA (GFA) maps from estimated orientation distribution functions. Using a deterministic tracking algorithm (EuDX; Garyfallidis et al., 2012) with standard tracking parameters (step size: 0.5mm, turning angle 45°, alpha = 0.05). Whole-brain streamlines (~30,000 per subject) were saved for subsequent parcellation into structural connectivity matrices (see below). Streamlines were filtered out if the two terminal points were located in the two node regions. Because a larger region is more likely to generate a larger number of streamlines, this fiber-density weighted network (Zhong et al., 2015) was corrected for nodal size $M_{i,j} = (2 \times FN)/(n_i + n_j)$, where n_i and n_j denote the number of voxels in regions *i* and *j*, respectively, and FN denotes the fiber number linking region *i* and region *j* (Cheng et al., 2012). Lastly, we corrected for spurious node pairs using a correction method described previously (Gong et al., 2009), in which a nonparametric sign-test was applied by taking each individual as

a sample, with the null hypothesis being that there is no existing connection, and a node pair surviving a corrected $p < 0.05$ was deemed to have a connection; all node pairs below this threshold were excluded from subsequent analyses.

Functional connection matrices representing task-related connection strengths were estimated using a correlational psychophysical interaction (cPPI) analysis (Fornito et al., 2011). Briefly, the model relies on the calculation of a PPI regressor for each region, based on the product of that region's timecourse and a task regressor of interest, in order to generate a term reflecting the psychophysical interaction between the seed region's activity and the specified experimental manipulation. In the current study the task regressors based on the convolved task regressors from the univariate model described above were used as the psychological regressor, which coded subsequently remembered and subsequently forgotten word pairs with positive and negative weights, respectively, of equal value. This psychological regressor was multiplied with two network timecourses for region i and j. We then computed the partial correlation $\rho_{PPI_i,PPI_j \cdot z}$, removing the variance z associated with the psychological regressor, the timecourses for regions i and j, and constituent noise regressors. We accounted for the potential effects of head motion and other confounds by assessing the 6 motion parameters and including these parameters in our partial correlation between regions.

Graph Theory Metrics

The graph theoretic approach used in the current manuscript focuses on two key mechanistic concepts: modularity and degree. Degree is a basic graph-theoretic measure describing the sum of edges at a node i in weighted networks, while modularity is a measure originally derived for quantifying the quality of a partition (Newman and Girvan, 2004), but more recently has become a key graph metric for quantifying the

relationship both within and between subnetworks in the whole-brain graph A. Fundamental to the definition of modularity is the computation of a proper null network, i.e. a null network, R, with the same number of nodes and node degrees but otherwise no underlying structure. If a natural division of a network exists, we should expect within-module connections between node i and j (A_{ij}) to be stronger than a random network R_{ij}, and connections between modules should be weaker than the same random network. Thus, modularity is higher the more partitioned a network is into modules that are densely connected within rather than between themselves. For a given partition of nodes of a network into modules, the modularity Q of this partition is

Eqn. 1.

$$Q = \frac{1}{2m} \sum_{i,j} \left(A_{ij} - R_{ij}\right) \delta(C_i, C_j)$$

where m C_i indicates group membership of node i. Therefore, modularity increases when $A_{ij} - R_{ij}$ (edge strength minus expected edge strength) is positive for within-module edges. Standard modularity analysis defines the null distribution (i.e., R_{ij}) from a randomization of the rows of the input matrix (Newman, 2006). However, even random networks can exhibit high modularity because of incidental concentrations of edges. This method of computing the null is also problematic for our analysis because it ignores negative connection weights and implicitly assumes self-loops (connections from nodes to themselves), which are meaningless in the functional networks considered here. Furthermore, modularity partitions based on randomized null distributions suffer from inconsistency in partition assignments over repeated executions of the same algorithm, and rely instead on permuting the algorithm for the maximum Q. We therefore employ a more recently developed modularity algorithm (Chang et al., 2014) that relies on a transformed Tracy-Widom distribution in order to more adequately model the null

distribution in a modularity computation, linking standard module detection with random matrix theory. Lastly, in order to compare functional and structural networks we use graph-theoretical methods to find the lowest weighted path in a structural network, which is constructed by connecting each cortical region with a weighted edge. The weights are defined such that paths that follow the principal diffusion direction have low weight.

Within-Module and Between-Module Degree

Generally, the sum, of edges, or connections between a node and other nodes in the network, defines the node's degree. We examined whether the distribution of node degree values, either within or between a set of cortical modules, differed between successful and unsuccessfully encoded trials. Following previous studies focusing on degree (Guimera and Nunes Amaral, 2005), for each participant in each condition we fit the degree distribution using an exponentially truncated power law function, P(k) ~ Aka-1ek/kc. From these fits, we extracted values for the power law exponent (a), exponential cutoff point (kc), and coefficient (A), and evaluated those parameters between encoding trilals which were subsequently remembered or forgotten, in both post-rTMS conditions (1Hz and 5Hz rTMS). Critically, we considered these changes in degree distribution at each node either with respect to its surrounding module (within-module degree or WMD), or as a function of a node's relationship with more distant cortical modules (between-module degree or BMD). Both WMD and BMD use the same underlying function to estimate degree:

Eqn. 2

$$z_i = \frac{\kappa_i - \kappa_{S_i}}{\sigma_{K_{S_i}}}$$

where κ_{S_i} is the average of K over all the nodes in S_i, and $\sigma_{K_{S_i}}$ is the standard deviation of κ. in S_i. This within-module degree z-score ($z_{i_{WMD}}$) measures how well connected node i is to other nodes within the module, while the between-module degree z-score ($z_{i_{BMD_m}}$) measures how well connected a node i is to other nodes with another module M in the cortical parcellation. As such, the calculation of $z_{i_{BMD}}$ is repeated for each module. In typical applications, nodes with a high z_{WMD} are interpreted to represent local, intramodular information-processing hubs, whereas nodes with high z_{BMD} show a relatively even distribution of connectivity across all modules (Fornito et al., 2012).

Cross-modal comparisons

Lastly, we sought to test the hypothesis that the regions that are most affected by rTMS stimulation are best predicted by the structural connectivity with the stimulation site. While a number of recent analyses have focused on first-order correlations between a structural connectivity matrix $\boldsymbol{A_{DTI}}$ and a functional connectivity matrix $\boldsymbol{A_{fMRI}}$, for a given region *R*, based on the assumption that direct structural connectivity should engender a corresponding modulation of functional connectivity (Zimmermann et al., 2016). However, there are typically large differences in sparsity between functional and structural connectivity networks, which make such an assumption untenable. Nonetheless, methods from spectral graph theory have emerged to estimate the relationship between pairs of regions in a structural connectivity matrix that are not connected by direct (i.e., 1-step) connections. The agreement of functional and structural connectivity between all regions was calculated using a novel method of estimating the functional-structural relationship as a function of the structural path length in a structural matrix $\boldsymbol{A_{DTI}}$. As described in Figure 2, we varied the maximum length of the paths under consideration in order to test whether the as a function of how directly it was connected

to the stimulation site. For a given structural connectivity matrix S, the *k*-th path length of S accounts for structural path lengths of length *k* connecting different brain parcels. In order to construct path length, we relied on Dijkstra's algorithm, which solves the single-source shortest path problem: given a weighted graph G = (V,E), where V is a set of vertices and E a set of edges, find a shortest path from a given source vertex s < V to every vertex v < V. A shortest path is defined as a path of which the sum of the weights of its edges is minimal. As such, the input to this algorithm is a connection-length matrix generated in each subject and adjusted to values between 0 and 1. In order to enhance the effect of high connection weights (i.e., streamline counts) with respect to low values we use a nonlinear decreasing function S to map streamline count C to edge weight, $W_{i,j} = S(C_{i,j})$. Following Everts et al. (2015), we use a decreasing sigmoidal function of the form

Eqn. 3

$$S(x) = \frac{1}{1 + e^{a(x-b)}}$$

where a is a positive constant that determines the steepness of the sigmoid and b is a constant that determines the x-position of the steepest point of S.

We then calculated the Pearson's product moment correlation between a vector describing the structural connectivity matrix at step size *k* (v_{DWI_k}) and a vector describing the functional connectivity v_{fMRI}; given the role of negative correlations described above, we used the absolute value of the functional connectivity information for each condition. This cross-modal correlation was then repeated for functional and structural connectivity weights at each cortical region, using only the vector describing connectivity from that site. Statistical significance in both global and region-specific relationships were obtained by Fisher-transforming the *r*-values obtained for each subject and calculating one-sample t-tests over the group.

Results

Behavioral performance

Concurrent with fMRI, participants repeatedly encoded sentences which each constituted a consistent grammatical structure; noun pairs from these sentences were then presented immediately afterwards in the subsequent retrieval session, with noun pairs either intact or recombined from two different sentences within the block. 5Hz- vs. 1Hz-frequency TMS did not alter behavioral performance, consistent with our intended use of TMS as a physiological probe (Clapp et al., 2010; Feredoes et al., 2011). Performance on the memory task for both baseline, excitatory, and inhibitory conditions is summarized in **Table 1**. Paired t-tests between baseline and TMS conditions demonstrated a no significant difference between baseline and 5Hz rTMS conditions (t_{12} = 2.02, p = 0.06), but no significant difference between baseline memory performance and 1Hz rTMS (t_{12} = 1.99, p = 0.08), or between 1Hz and 5Hz rTMS conditions (t_{12} = 0.53, p = 0.6). No significant differences were observed between stimulation conditions for response times, for either successfully remembered or forgotten trials.

Table 1. Behavioral results.

Accuracy	**Hit Rate (SE)**		**False Alarm Rate (SE)**		**d' (SE)**	
Baseline	0.77	0.04	0.18	0.07	1.97	0.31
1Hz rTMS	0.82	0.04	0.12	0.02	2.35	0.21
5Hz rTMS	0.85	0.03	0.13	0.03	2.46	0.27
Response Time	**H (SE)**		**FA (SE)**			
Baseline	1835	130	2318	120		
1Hz rTMS	1644	50	2425	94		
5Hz rTMS	1549	94	2243	105		

Given the differences in connectivity described below, one possible explanation for this null finding is that the detrimental effects of 1Hz rTMS were counteracted by an

increase in distributed processing; we examine this hypothesis in more detail below. The focus of the present study is not to necessarily elicit a behavioral benefit, but to examine the functional network dynamics in response to stimulation. As such, the remaining analyses focus on the functional and structural dynamics supporting this consistent level of functioning under either inhibitory or excitatory stimulation conditions.

Univariate fMRI results

In order to confirm that our stimulation conditions (baseline, 5Hz, 1Hz stimulation) had a reliable effect on local LMFG activity, we conducted a series of univariate models to explain the subsequent-memory effect (SME) in this a priori region of interest. **Figure 3** describes the SME in each of our three experimental conditions (baseline, 1Hz, and 5Hz conditions); we focus here on the left MFG target site, which demonstrates both 1) a baseline SME on Day 1 (thus making it a consistent TMS target), 2) depressed activity after 10 minutes of 1Hz rTMS, and 3) increased activity after 10 minutes of 5Hz rTMS. The spatial extent of the SME-related activity in all 3 conditions was very similar; additional peaks of activity are reported in **Table 2**.

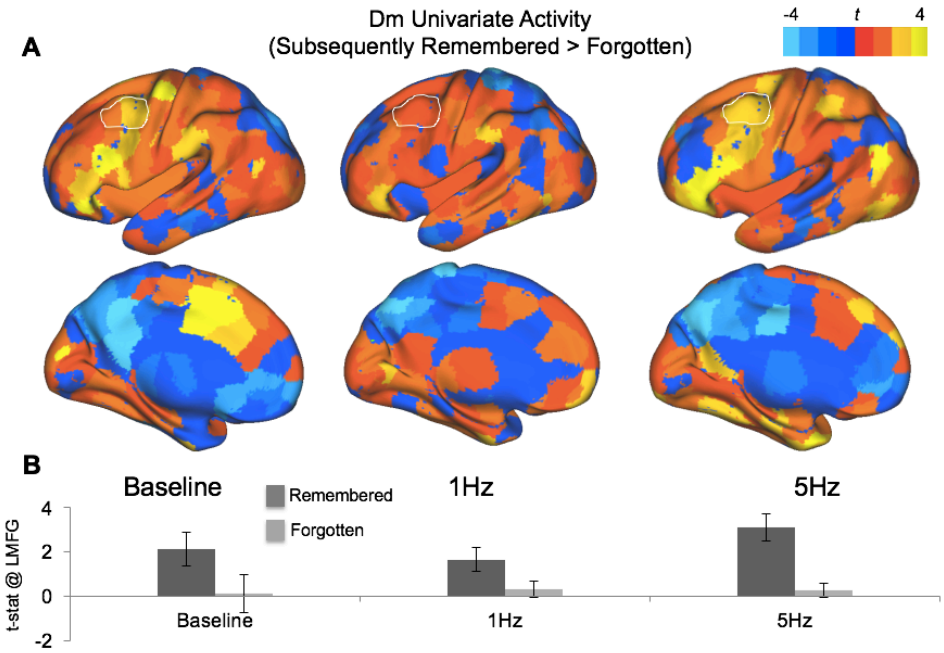

Figure 3. Univariate effects at stimulation site. Maps of Difference due to memory (Dm) effects in all 471 cortical ROIs mapped onto the left hemisphere with lateral and medial views (A); the left MFG stimulation site overlap across all participants is outlined in white. (B) describes the one-sample t-statistic for subsequently remembered or forgotten trials.

Multivariate Network Analyses

Our main analysis focused on the effects of excitation and inhibition the modular structure of memory success-related networks in the aging brain. We used 5Hz and 1Hz rTMS in order to enable a causal assessment of the stimulated brain region's influence on connected brain regions, which we evaluate by summarizing the effects on the modular structure of success-related brain activity.

Network modularity across conditions

We next sought to establish a consistent modular structure based on the success-related network defined in absence of any effects of stimulation. We constructed a group average from based on subsequent memory connectivity during the baseline (Day 1) condition, and applied a data-driven algorithm for identifying consistent module partitions

(Chang et al., 2012). Baseline modularity assignments are represented in **Figure 4A**, which show a clear demarcation between 5 networks: left and right PFC modules, a bilateral temporal module, a posterior occipital-parietal module, and a module comprising nodes from the cerebellar network.

To understand the functional roles played by each module and their constituent nodes, we examined two key metrics related the degree distribution at a given node either within that node's module (within module degree, or WMD) or between that node and all other nodes with any of the other modules identified above (between-module degree, or BMD). We first examined changes in z_{WMD} scores between successfully remembered or forgotten encoding trials (i.e., the Dm contrast), during either 1Hz or 5Hz stimulation. **Figure 4B** describes the success-related increases in z_{WMD} with the application of 1Hz and 5Hz stimulation, respectively, at each ROI. After 1Hz rTMS, few regions emerged, including 2 ROIs in left occipital cortex, portions of the right angular gyrus, (all $t_{12} > 2$). We found no success related effects on WMD during the 1Hz condition in left PFC. In contrast, after 5Hz rTMS, a number of regions demonstrated Dm effects, including included the stimulation site, LMFG ($t_{12} = 4.17$, $p < 0.005$), RSFG ($t_{12} = 2.46$, $p < 0.005$), R inferior frontal gyrus-operculum ($t_{12} = 3.84$, $p < 0.005$), L Superior Orbital cortex ($t_{12} = -3.40$, $p < 0.005$), and bilateral posterior cingulate regions. The directionality of these effects suggests that both positive and negative connection strengths contribute to successful memory performance, and justify the inclusion of negative connection weights in this and preceding modularity analyses. In contrast, 5Hz stimulation was associated with large increases in WMD in multiple PFC and temporal regions, including the LMFG stimulation site ($t_{12} = 2.28$, $p < 0.05$) and its contralateral homologue ($t_{12} = 2.12$, $p < 0.05$), as well as ipsilateral angular gyrus ($t_{12} = 2.78$, $p < 0.01$) and right hippocampus ($t_{12} = 2.36$, $p < 0.01$).

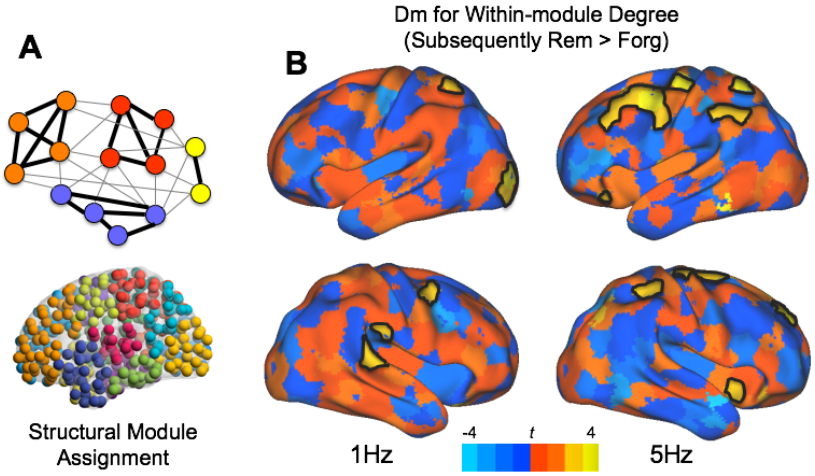

Figure 4. Within-Module Degree associated with subsequent memory across rTMS conditions. Modularity defined by structural connectivity (A) describes a discrete network of left and right PFC modules, and premotor, motor, temporal, and occipital modules. An examination of the within-module degree (B) for each ROI suggests greater local (left PFC) processing in the 5Hz condition. Statistically significant regions ($p < 0.05$) are outlined in black.

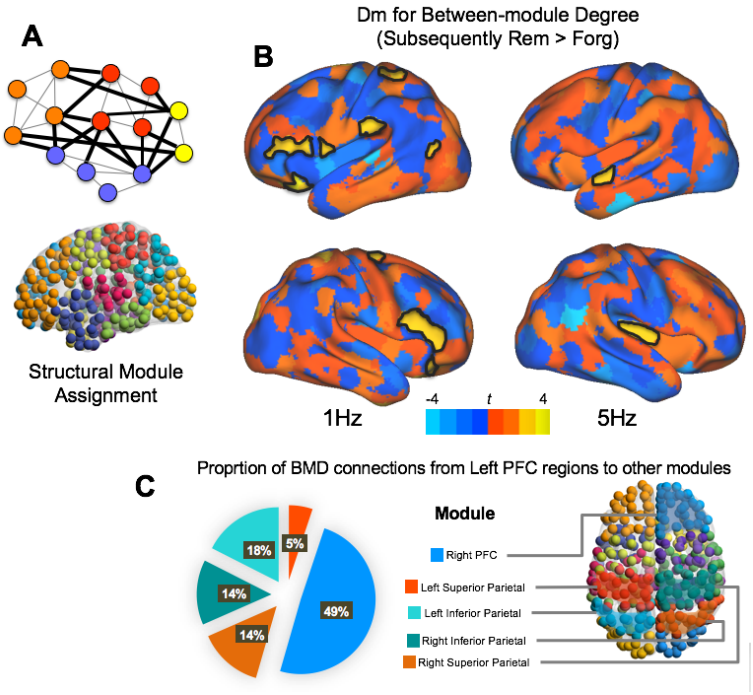

Figure 5. Between-Module Degree associated with subsequent memory across rTMS conditions. Turning to Between-Module Degree (BMD), we use the same modularity defined by structural connectivity

as above (A) in order to define effect sizes describing greater BMD for successfully remembered than forgotten trials. While connectivity after 5Hz stimulation demonstrates no PFC effect, BMD values in the 1Hz stimulation condition emerge in left and right PFC are greater for successful trials, suggesting that 1Hz stimulation is associated with more intermodular, global communication (B). A more careful analysis of these between module connections in the 1Hz condition (C) demonstrates that this increase in success-related BMD is largely attributable to a higher proportion of connectivity to contralateral Right PFC module (which also shows a success-related increase in BMD See Figure 5B). Statistically significant regions ($p < 0.05$) are outlined in black.

Turning to between-module degree, we found a constrained set of regions that demonstrated greater connectivity during successfully remembered than forgotten trials in bilateral PFC after 1Hz—but not 5Hz rTMS (**Figure 5)**. Regions associated with memory success after 5Hz rTMS were limited to a region in the left anterior superior temporal gyrus ($t_{12} = 3.15$, $p < 0.01$) and right Heschel's gyrus ($t_{12} = 3.45$, $p < 0.01$). Conversely, we found a significant effect of Success in 4 left PFC ROIs (all ROIs $p < 0.05$) and 3 right PFC ROIs after 1Hz rTMS. Posthoc assessments of the z_{BMD} between the left-hemisphere cluster of regions and all other modules revealed that the greater BMD Dm effect was largely due to the increase in degree with contralateral ROIs in the MFG (mean z_{BMD} to right PFC module = 3.35; to all other modules < 1.0). Though these sites were not directly stimulated by rTMS, they nonetheless share strong structural connectivity with the target LMFG site. Lastly, we examined which modules contribute to this BMD increase (**Figure 5C**), and found that the proportion of between-module connections in the 1Hz condition is largely attributable to a higher proportion of connectivity to contralateral Right PFC module (49% of all significant between-module connections with left PFC regions), which also shows a success-related increase in BMD). Modules comprising bilateral parietal cortex also contributed significantly to the left PFC BMD effect (Left Superior Parietal: 5%; Right Superior Parietal: 14%; Left Inferior Parietal: 18%; Right Inferior Parietal: 14%). These results suggest that the aging

brain utilizes a flexible, cross-module network including bilateral PFC and parietal regions in order to maintain successful memory performance.

Lastly, in order to explore the hypothesis that stimulation-induced changes in functional degree compensate for a deficit in core network regions, by relying on between module connections (BMD) when local resources are depleted through 1Hz rTMS. Indeed, we found a reliable negative correlation across subjects (r_{12} = -0.21), across all left PFC nodes, between univariate fMRI activity and BMD during successful trials (Hits), which was absent during misses (**Figure 6**). This effect was selective for the 1Hz rTMS condition, during which the local subsequent memory effect in fMRI univariate activity was attenuated (see **Figure 3**), and was not present after 5Hz rTMS, which had the opposite effect on local fMRI activity. No such relationships were observed in the relationship between univariate activity and WMD (all $r < 0.05$).

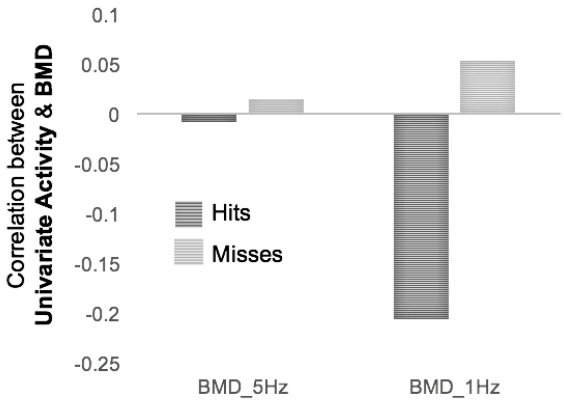

Figure 6. Relationship (Pearson's r) between left PFC univariate success activity (Hits > Misses) and connectivity between the left PFC module and all other modules.

Cross-modal comparison

Lastly, we sought to quantify the relationship between structural connectivity based on streamline tractography, and functional connectivity, based on task-based connectivity. We quantified the relationship between structural connectivity strength and success-related functional connectivity in our 3 rTMS conditions (baseline, 5Hz, and 1Hz). R-

values were relatively high across conditions and ROIs, suggesting a general coupling between functional and structural connectivity (Honey et al., 2009). We varied the maximum length of the paths under consideration in order to test whether the as a function of how directly it was connected to the stimulation site. For a given structural connectivity matrix *S*, the *k*-th path length of *S* accounts for structural path lengths of length *k* connecting different brain parcels **Figure 7**. Given the a priori interest in left MFG rTMS target, we focused on the distribution of structure-function correlations (r-values) for this region (center of mass = [-45, 18, 40]) within the left PFC module. Following a significant Condition x Maximum Path Length interaction ($F_{3,460} = 12.51$, $p < 0.05$), pairwise t-tests revealed that these relationships were stronger for functional networks based on data collected after 5Hz than during the baseline condition at path length 1 ($t_{12} = 2.46$, $p < 0.05$). Conversely, stronger structure-function relationships emerged for 1Hz networks at longer path lengths (4 & 5) ($t_{12} = 2.42, 2.75$, respectively, both $p < 0.05$).

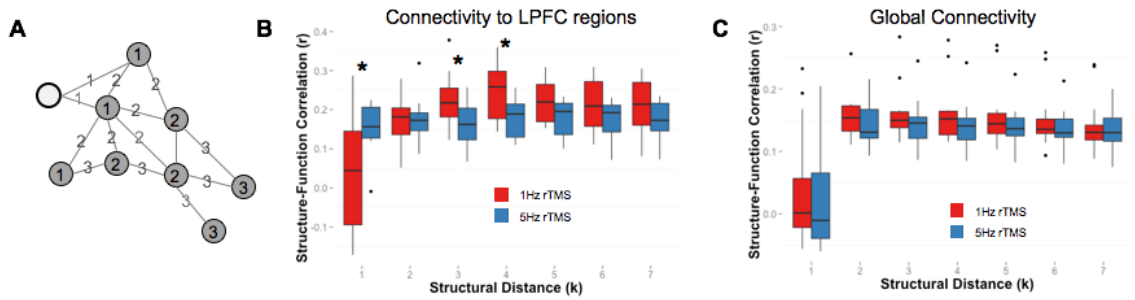

Figure 7. Structure-function relationships. We represent the evolution of the correlation quality between structural (defined by diffusion tractography) and functional (defined by cPPI) connectivity matrices at multiple dimensionality (defined by Maximum path length). As such, we define the path length as the number of steps between two ROIs (**A**), as defined by the structural graph. (**B**) We found that this function-structure relationship was strong (mean r > 0.45 in all conditions/lengths). Pairwise t-tests revealed that these relationships were stronger for functional networks based on data collected after 5Hz than during the baseline condition at path length 1, while this relationship was stronger for 1Hz networks at longer path lengths (3 & 4). (**C**) An examination of these relationships at the global level suggests no such frequency-specific modulation.

Based on these results, we can quantify the importance of structural paths of different lengths in predicting the hemodynamic response to rTMS at a localized PFC region. For example, at k = 1 we see a significantly stronger relationship between structural connectivity and functional connectivity in $\boldsymbol{F_{5Hz}}$ than in $\boldsymbol{F_{1Hz}}$; thus, we can conclude that success-related connectivity after 5Hz stimulation is more reliant on direct structural paths. The value of higher order connections (k = 3,4) is more predictive of functional connectivity in $\boldsymbol{F_{1Hz}}$ than in $\boldsymbol{F_{5Hz}}$; suggesting that 1Hz-related connectivity is more dependent on more indirect structural connectivity. An examination of these effects outside of the left PFC, incorporating all regions, demonstrates no frequency-selective modulation of the structure-function relationship at any step size. These effects describe an overall pattern consistent with our modularity results above, such that stimulation-related increases in local connectivity (i.e., WMD) after 5Hz rTMS, and increases in global connectivity (i.e., BMD) following 1Hz rTMS, were both constrained by short- and long-distance topology (respectively).

Discussion

In order to assess how PFC reorganization benefits the aging brain, we studied the influence of local 1Hz and 5Hz rTMS over the left MFG on whole brain, task-based connectivity. The study yielded two main findings. First, modular network features of success-related network connectivity showed qualitatively different patterns, with 5Hz stimulation associated with over-activation at the stimulation site and an increase in within-module degree, while 1Hz rTMS was associated with under-activation at the stimulation site and an increase in between-module degree to contralateral PFC and parietal modules. Second, we found that these patterns were constrained by diffusion-weighted tractography from the stimulation site in a manner consistent with our fMRI

findings, such that the relationship between success-related functional connectivity and structural connectivity was stronger between 5Hz functional connectivity and shorter white-matter tracts, and between 1Hz functional connectivity and longer white-matter tracts. We discuss these two findings below.

A critical finding from the current analysis is that 5Hz stimulation to a memory-specific target was associated with greater within-module connectivity (WMD), while 1Hz rTMS engendered a more distributed pattern of connectivity with other modules (BMD). This finding is consistent with our hypothesis that widespread activity patterns observed in OA populations during similar memory encoding tasks reflect a shift from local to global network activity in order to compensate for local deficits. While typical assessments of these patterns are made across cohorts of younger and older adults, the current results represent a novel means of probing aging brain function by using a frequency-specific changes in cognitive and network state. Furthermore, when examining the subject-wise relationship between activity and BMD connectivity, we found that post-1Hz rTMS BMD engendered such a compensatory relationship (**Fig. 6**), such that TMS-induced declines in fMRI activity during Hits were inversely related to increases in more distal BMD connectivity. This result suggest that OAs compensate for the depletion of local resources by relying on a more distributed pattern of connectivity.

A number of recent analyses have demonstrated that both weak intramodular connections and more distant, intermodular connections play a crucial role in transforming the brain from its modular structure (Gallos et al., 2012; Santarnecchi et al., 2014; Geerligs et al., 2015). Age-related examinations of these network properties have typically relied on resting brain activity, and generally describe a decline in the network cohesion (i.e., modularity) when compared with younger counterparts (Betzel et al., 2014; Cao et al., 2014). However, growing evidence in task-related studies of whole-brain connectivity suggests that, despite this reduction in functional specificity, older

adults are able to adapt the functional connectivity between functional networks (or modules) in order to adapt to task demands (Geerligs et al., 2014a; Geerligs et al., 2014b; Meunier et al., 2014). We connect this nascent literature with a more established set of findings based on general observation of univariate age-related increases and decreases in PFC activity in relationship to a cognitive task. Furthermore, we stress therefore that a more mechanistic understanding of how the aging brain adjusts to brain stimulation is necessary before the therapeutic use of a noninvasive brain stimulation method is considered as a practical application in a normative elderly population. We observed changes in network organization in absence of behavioral changes in either 1Hz or 5Hz stimulation conditions; focusing on changes in functional activity (or connectivity) *in absence* of a behavioral TMS effect (e.g., Clapp et al., 2011) is a key first step in the identification of adaptable age-related reorganization.

The impact of TMS on neural functioning in aging populations during memory tasks is still in its infancy. Nonetheless, new consensus is building towards the specific stimulation parameters that engender a positive effect on cognitive function in physiological and pathological aging (for review, see Hsu et al., 2015). Disruptive brain stimulation experiments which in high-performing older adults (Brambilla et al., 2015) suggest a positive role for the age-related increase in bilateral engagement of dorsolateral PFC regions during episodic memory tasks. In line with these studies, we showed that stimulation-induced reductions in local activity after 1Hz rTMS resulted in increased connectivity between left and right PFC, suggesting a frequency-specific role for this type of network reorganization. As noted above, frequency-specific TMS can selectively alter intrinsic neural dynamics between and within functionally specialized large-scale brain modules. This hypothesis is supported by the results of empirical and simulation studies, which suggest that the functional effects of focal changes in neural activity may extend outside a functionally segregated network (Bestmann et al., 2004;

Alstott et al., 2009; van Dellen et al., 2013). Because large-scale modules are positioned at an intermediate scale between local and global integration, they may play a critical role in integrating local changes without reorganizing the backbone of large-scale brain communication. Nonetheless, the most effective parameters and dosing of stimulation (i.e., stimulation tool, frequency of rTMS, intensity, number of rTMS pulses, target brain region) in aging populations demands further investigation.

Turning to our cross-modal network analysis, we found that the structural networks given by diffusion-weighted tractography reliably constrained the functional connectivity. We found that while direct paths best correlate with functional networks derived from the post-5Hz fMRI. In contrast, the more indirect (3rd- and 4th-step) structural networks more strongly predicted 1Hz success networks. This pattern of results mirrors our earlier WMD/BMD findings, suggesting that both global, between-module connectivity patterns are constrained by structural connectivity. This result offers a clear, mechanistic explanation for the anatomical basis for localizing the effects of changes at a proximal site at more distant locations in the aging brain. While regional correlations between diffusion based structural connectivity and task-based functional connectivity remained consistently above chance—reflecting a general trend than structural connectivity may help explain some, but not all of the variance in functional connectivity (Honey et al., 2009; Betzel et al., 2014)—this relationship was most pronounced in the connections emanating from the stimulation site.

These cross-modal findings, taken together, have two implications. First, given the population from which these relationships were derived, these results build towards the growing that structural networks are a critical component in older adults' ability to flexibly adapt to novel task conditions (Gold et al., 2010; Daselaar et al., 2013). Second, this finding has important clinical implications, as many of the sites inaccessible to TMS

may be accessed via structural or functional connectivity (Fox et al., 2014) once we understand the network influence of focal stimulation and its downstream impact.

Limitations

While the above findings provide a clear causal role for the role of bilateral brain dynamics in shaping healthy performance, the current analysis nonetheless suffers principally from two major limitations: a low sample size and a design that limits the interpretation of TMS-specific effects. With respect to the former limitation, the issue is whether the observed results might generalize to a broader aging population, or in fact is unique to older adults in the first place. It is important to note that although our hypothesis and two predictions mention OAs, they are not specific to aging. On the contrary, we believe the hypothesis that brain decline can be compensated with a shift from WMC to BMC would also apply with YAs suffering of brain dysfunction due to lesions or transient TMS effects. Thus, we could have investigated the hypothesis and predictions in either OAs or YAs. Nonetheless, we highlighted the advantage of the multimodal nature of our dataset, and nonetheless believe this unique contribution suggests further studies designed with our results in mind. With respect to the latter limitation, we focused on elucidating a frequency-specific change in brain state (5Hz and 1Hz) in order to compare their effects on network organization in the aging brain, based on work from our own (Luber et al., 2007; Luber et al., 2008) and other laboratories which have found both fMRI-based (Schneider et al., 2010) and MEP-based evidence that 5Hz rTMS promotes increases in cortical excitability (Peinemann et al., 2004). While our rTMS design lacked a same-day sham condition to eliminate the possibility that performance differences due to the arousing effects of TMS, neuroenhancement as such was not the goal of the present analysis. Our fMRI findings nonetheless support

important distinctions between rTMS parameters, and suggest important frequency-specific effects on global network organization.

Conclusions

The current analysis provides novel evidence that aging brains utilizes a flexible set of neural dynamics to accomplish the same cognitive task under different Stimulation conditions. Local 5Hz stimulation engendered an increase in local connectivity (WMD) related to successful memory performance, while the application of 1Hz rTMS engendered more global connectivity (BMD) to different brain modules located bilaterally from the site of stimulation. These more global effects were strongly constrained by structural connectivity derived from diffusion-weighted tractography. These results provide an integrated, causal explanation of the network interactions associated with successful memory encoding in older adults.

References

Alstott J, Breakspear M, Hagmann P, Cammoun L, Sporns O (2009) Modeling the impact of lesions in the human brain. PLoS computational biology 5:e1000408.

Antonenko D, Meinzer M, Lindenberg R, Witte AV, Floel A (2012) Grammar learning in older adults is linked to white matter microstructure and functional connectivity. Neuroimage 62:1667-1674.

Bellec P, Benhajali Y, Carbonell F, Dansereau C, Albouy G, Pelland M, Craddock C, Collignon O, Doyon J, Stip E, Orban P (2015) Impact of the resolution of brain parcels on connectome-wide association studies in fMRI. NeuroImage.

Bestmann S, Baudewig J, Siebner HR, Rothwell JC, Frahm J (2004) Functional MRI of the immediate impact of transcranial magnetic stimulation on cortical and subcortical motor circuits. Eur J Neurosci 19:1950-1962.

Betzel RF, Byrge L, He Y, Goni J, Zuo XN, Sporns O (2014) Changes in structural and functional connectivity among resting-state networks across the human lifespan. Neuroimage 102P2:345-357.

Brambilla M, Manenti R, Ferrari C, Cotelli M (2015) Better together: Left and right hemisphere engagement to reduce age-related memory loss. Behav Brain Res 293:125-133.

Cao M, Wang JH, Dai ZJ, Cao XY, Jiang LL, Fan FM, Song XW, Xia MR, Shu N, Dong Q, Milham MP, Castellanos FX, Zuo XN, He Y (2014) Topological organization of the human brain functional connectome across the lifespan. Dev Cogn Neurosci 7:76-93.

Chang YT, Leahy RM, Pantazis D (2012) Modularity-based graph partitioning using conditional expected models. Phys Rev E Stat Nonlin Soft Matter Phys 85:016109.

Chang YT, Pantazis D, Leahy RM (2014) To cut or not to cut? Assessing the modular structure of brain networks. NeuroImage 91:99-108.

Clapp WC, Rubens MT, Gazzaley A (2010) Mechanisms of working memory disruption by external interference. Cereb Cortex 20:859-872.

Clapp WC, Rubens MT, Sabharwal J, Gazzaley A (2011) Deficit in switching between functional brain networks underlies the impact of multitasking on working memory in older adults. Proceedings of the National Academy of Sciences of the United States of America 108:7212-7217.

Cox SR, Bastin ME, Ferguson KJ, Allerhand M, Royle NA, Maniega SM, Starr JM, MacLullich AM, Wardlaw JM, Deary IJ, MacPherson SE (2015) Compensation or inhibitory failure? Testing hypotheses of age-related right frontal lobe involvement in verbal memory ability using structural and diffusion MRI. Cortex; a journal devoted to the study of the nervous system and behavior 63:4-15.

Daselaar SM, Iyengar V, Davis SW, Eklund K, Hayes SM, Cabeza RE (2013) Less Wiring, More Firing: Low-Performing Older Adults Compensate for Impaired White Matter with Greater Neural Activity. Cereb Cortex.

Davis SW, Kragel JE, Madden DJ, Cabeza R (2012) The architecture of cross-hemispheric communication in the aging brain: linking behavior to functional and structural connectivity. Cereb Cortex 22:232-242.

Davis SW, Zhuang J, Wright P, Tyler LK (2014) Age-related sensitivity to task-related modulation of language-processing networks. Neuropsychologia 63:107-115.

de Vries PM, de Jong BM, Bohning DE, Hinson VK, George MS, Leenders KL (2012) Reduced parietal activation in cervical dystonia after parietal TMS interleaved with fMRI. Clin Neurol Neurosurg 114:914-921.

Dennis NA, Hayes SM, Prince SE, Madden DJ, Huettel SA, Cabeza R (2008) Effects of aging on the neural correlates of successful item and source memory encoding. J Exp Psychol Learn Mem Cogn 34:791-808.

Everts MH, Begue E, Bekker H, Roerdink JB, Isenberg T (2015) Exploration of the Brain's White Matter Structure through Visual Abstraction and Multi-Scale Local Fiber Tract Contraction. IEEE Trans Vis Comput Graph 21:808-821.

Feredoes E, Heinen K, Weiskopf N, Ruff C, Driver J (2011) Causal evidence for frontal involvement in memory target maintenance by posterior brain areas during distracter interference of visual working memory. Proceedings of the National Academy of Sciences of the United States of America 108:17510-17515.

Fornito A, Harrison BJ, Zalesky A, Simons JS (2012) Competitive and cooperative dynamics of large-scale brain functional networks supporting recollection. Proc Natl Acad Sci U S A 109:12788-12793.

Fornito A, Yoon J, Zalesky A, Bullmore ET, Carter CS (2011) General and specific functional connectivity disturbances in first-episode schizophrenia during cognitive control performance. Biol Psychiatry 70:64-72.

Fox MD, Buckner RL, Liu H, Chakravarty MM, Lozano AM, Pascual-Leone A (2014) Resting-state networks link invasive and noninvasive brain stimulation across diverse psychiatric and neurological diseases. Proc Natl Acad Sci U S A 111:E4367-4375.

Gallos LK, Makse HA, Sigman M (2012) A small world of weak ties provides optimal global integration of self-similar modules in functional brain networks. Proc Natl Acad Sci U S A 109:2825-2830.

Garyfallidis E, Brett M, Correia MM, Williams GB, Nimmo-Smith I (2012) QuickBundles, a Method for Tractography Simplification. Frontiers in neuroscience 6:175.

Garyfallidis E, Brett M, Amirbekian B, Rokem A, van der Walt S, Descoteaux M, Nimmo-Smith I, Dipy C (2014) Dipy, a library for the analysis of diffusion MRI data. Frontiers in neuroinformatics 8:8.

Geerligs L, Maurits NM, Renken RJ, Lorist MM (2014a) Reduced specificity of functional connectivity in the aging brain during task performance. Hum Brain Mapp 35:319-330.

Geerligs L, Saliasi E, Renken RJ, Maurits NM, Lorist MM (2014b) Flexible connectivity in the aging brain revealed by task modulations. Hum Brain Mapp 35:3788-3804.

Geerligs L, Renken RJ, Saliasi E, Maurits NM, Lorist MM (2015) A Brain-Wide Study of Age-Related Changes in Functional Connectivity. Cereb Cortex 25:1987-1999.

Gold BT, Powell DK, Xuan L, Jicha GA, Smith CD (2010) Age-related slowing of task switching is associated with decreased integrity of frontoparietal white matter. Neurobiology of aging 31:512-522.

Gong G, He Y, Concha L, Lebel C, Gross DW, Evans AC, Beaulieu C (2009) Mapping anatomical connectivity patterns of human cerebral cortex using in vivo diffusion tensor imaging tractography. Cereb Cortex 19:524-536.

Guimera R, Nunes Amaral LA (2005) Functional cartography of complex metabolic networks. Nature 433:895-900.

Honey CJ, Sporns O, Cammoun L, Gigandet X, Thiran JP, Meuli R, Hagmann P (2009) Predicting human resting-state functional connectivity from structural connectivity. Proc Natl Acad Sci U S A 106:2035-2040.

Hsu WY, Ku Y, Zanto TP, Gazzaley A (2015) Effects of noninvasive brain stimulation on cognitive function in healthy aging and Alzheimer's disease: a systematic review and meta-analysis. Neurobiology of aging 36:2348-2359.

Luber B, Kinnunen LH, Rakitin BC, Ellsasser R, Stern Y, Lisanby SH (2007) Facilitation of performance in a working memory task with rTMS stimulation of the precuneus: frequency- and time-dependent effects. Brain Res 1128:120-129.

Luber B, Stanford AD, Bulow P, Nguyen T, Rakitin BC, Habeck C, Basner R, Stern Y, Lisanby SH (2008) Remediation of sleep-deprivation-induced working memory impairment with fMRI-guided transcranial magnetic stimulation. Cereb Cortex 18:2077-2085.

Meunier D, Stamatakis EA, Tyler LK (2014) Age-related functional reorganization, structural changes, and preserved cognition. Neurobiology of aging 35:42-54.

Nelson DL, McEvoy CL, Schreiber TA (2004) The University of South Florida free association, rhyme, and word fragment norms. Behav Res Methods Instrum Comput 36:402-407.

Newman ME (2006) Modularity and community structure in networks. Proc Natl Acad Sci U S A 103:8577-8582.

Nyberg L, Salami A, Andersson M, Eriksson J, Kalpouzos G, Kauppi K, Lind J, Pudas S, Persson J, Nilsson LG (2010) Longitudinal evidence for diminished frontal cortex function in aging. Proc Natl Acad Sci U S A 107:22682-22686.

Peinemann A, Reimer B, Loer C, Quartarone A, Munchau A, Conrad B, Siebner HR (2004) Long-lasting increase in corticospinal excitability after 1800 pulses of subthreshold 5 Hz repetitive TMS to the primary motor cortex. Clinical neurophysiology : official journal of the International Federation of Clinical Neurophysiology 115:1519-1526.

Persson J, Nyberg L, Lind J, Larsson A, Nilsson LG, Ingvar M, Buckner RL (2006) Structure-function correlates of cognitive decline in aging. Cereb Cortex 16:907-915.

Proskovec AL, Heinrichs-Graham E, Wilson TW (2016) Aging modulates the oscillatory dynamics underlying successful working memory encoding and maintenance. Hum Brain Mapp 37:2348-2361.

Santarnecchi E, Galli G, Polizzotto NR, Rossi A, Rossi S (2014) Efficiency of weak brain connections support general cognitive functioning. Hum Brain Mapp 35:4566-4582.

Schneider SA, Pleger B, Draganski B, Cordivari C, Rothwell JC, Bhatia KP, Dolan RJ (2010) Modulatory effects of 5Hz rTMS over the primary somatosensory cortex in focal dystonia--an fMRI-TMS study. Mov Disord 25:76-83.

Smith SM, Jenkinson M, Johansen-Berg H, Rueckert D, Nichols TE, Mackay CE, Watkins KE, Ciccarelli O, Cader MZ, Matthews PM, Behrens TE (2006) Tract-based spatial statistics: voxelwise analysis of multi-subject diffusion data. Neuroimage 31:1487-1505.

Spaniol J, Grady C (2012) Aging and the neural correlates of source memory: over-recruitment and functional reorganization. Neurobiology of aging 33:425 e423-418.

Spaniol J, Davidson PS, Kim AS, Han H, Moscovitch M, Grady CL (2009) Event-related fMRI studies of episodic encoding and retrieval: meta-analyses using activation likelihood estimation. Neuropsychologia 47:1765-1779.

Tzourio-Mazoyer N, Landeau B, Papathanassiou D, Crivello F, Etard O, Delcroix N, Mazoyer B, Joliot M (2002) Automated anatomical labeling of activations in SPM using a macroscopic anatomical parcellation of the MNI MRI single-subject brain. Neuroimage 15:273-289.

van Dellen E, Hillebrand A, Douw L, Heimans JJ, Reijneveld JC, Stam CJ (2013) Local polymorphic delta activity in cortical lesions causes global decreases in functional connectivity. Neuroimage 83:524-532.

Zhong S, He Y, Gong G (2015) Convergence and divergence across construction methods for human brain white matter networks: an assessment based on individual differences. Human brain mapping 36:1995-2013.

Zimmermann J, Ritter P, Shen K, Rothmeier S, Schirner M, McIntosh AR (2016) Structural architecture supports functional organization in the human aging brain at a regionwise and network level. Hum Brain Mapp.